Published for SISSA by Springer

Received: *February 6, 2015*
Accepted: *March 21, 2015*
Published: *April 15, 2015*

The NLO jet vertex in the small-cone approximation for kt and cone algorithms

D. Colferai and A. Niccoli

Dipartimento di Fisica e Astronomia, Università di Firenze and INFN, Sezione di Firenze, 50019 Sesto Fiorentino, Italy

E-mail: colferai@fi.infn.it, alessandro.niccoli@unifi.it

Abstract: We determine the jet vertex for Mueller-Navelet jets and forward jets in the small-cone approximation for two particular choices of jet algoritms: the kt algorithm and the cone algorithm. These choices are motivated by the extensive use of such algorithms in the phenomenology of jets. The differences with the original calculations of the small-cone jet vertex by Ivanov and Papa, which is found to be equivalent to a formerly algorithm proposed by Furman, are shown at both analytic and numerical level, and turn out to be sizeable. A detailed numerical study of the error introduced by the small-cone approximation is also presented, for various observables of phenomenological interest. For values of the jet "radius" $R = 0.5$, the use of the small-cone approximation amounts to an error of about 5% at the level of cross section, while it reduces to less than 2% for ratios of distributions such as those involved in the measure of the azimuthal decorrelation of dijets.

Keywords: Jets, NLO Computations

ArXiv ePrint: 1501.07442

doi:10.1007/JHEP04(2015)071

JHEP04(2015)071

Contents

JHEP04(2015)071

1 Introduction

The identification of high-energy (Regge) dynamics in QCD processes has been long since theoretically investigated. With the advent of high-energy colliders like HERA, Tevatron and LHC such studies have become possible at experimental level too. The processes which are expected to be more sensitive to this peculiar dynamical regime, where the center-of-mass energy $\sqrt{s}$ is much larger than all hard scales involved in the scattering, are the so-called *Mueller-Navelet* (MN) *jets* at hadron-hadron colliders [1] and *forward jets* at electron-hadron colliders [2, 3]. Both of them are defined by the presence of QCD jets at large rapidity, accompanied by any hadronic activity which is inclusively collected in the central region.

Such processes can be theoretically described by factorization formulae which involve several ingredients: the partonic distribution functions (PDFs) of the incoming hadron(s),

the gluon Green's function (GGF) describing the high-energy dynamics of emitted and exchanged partons — mostly (reggeized) gluons — and finally the so-called jet vertices, describing the production of a forward jet from the interaction of one incoming parton and a reggeized gluon. In the case of an incoming electron, an additional quantity, the photon impact factor, has to be considered too.

At present, all ingredients are known at next-to-leading level in the respective parameters: the PDFs which resum logarithms of collinear type, the GGF resumming logarithms of the energy, and the jet vertices (and impact-factors) which are computed at finite perturbative order.

Focusing for definiteness on MN jets in hadron-hadron collision, the process-dependent part of the cross section is represented by the jet vertex [4, 5], which depends on the jet variables and the actual jet algorithm. By following the work of Ivanov and Papa [6], in this paper we reconsider the computation of the jet vertex in the small-cone approximation (SCA), namely for jets whose extension in the rapidity-azimuthal angle (y, ϕ)-plane is small. In particular we apply their method to determine the analytic expressions of the jet vertex for two particular choices of jet algorithms: the *kt algorithm*[1] [7] and the *cone algorithm* [8]. These are the mostly used algorithms in modern jet phenomenology, in particular the kt one. On the contrary, the algorithm used in [6] can be traced back to the one considered by Furman [9] in early studies of QCD radiation, but not used for practical purposes anymore, being infra-red unsafe.

The aim of our work is twofold: on one hand we want to give a precise estimate of the error introduced by the small-cone approximation in the description of QCD observables at high energies, i.e., at large rapidities, so as to possibly justify its use in phenomenological analyses. On the other hand, we want to estimate the differences occurring by choosing different jet algorithms for the same process. The jet algorithm dependence has already been studied in the past, and a detailed analysis of the cone and kt algorithms in the SCA was presented in ref. [10, 11] in the context of collinear factorization. Here we carry out a similar analysis in the framework of high-energy (kt-dependent) factorization, the basic tool for the description of the Regge regime in perturbative QCD.

One should keep in mind that the small-cone expressions are fully analytic (before their convolution with the PDFs) and compact, and allow a simple implementation in numerical codes that run much faster than those with the exact jet vertices. For this reason the SCA jet vertices have already been used [12, 13] in quantitative comparison with available data [14]. However, the experimental results were extracted by clustering jets with the kt algorithm, while the SCA jet vertices used for the theoretical calculation were those obtained with the Furman algorithm by Ivanov and Papa (FIP). Also the small-cone analysis performed in ref. [15] compared calculations with the exact jet vertices in the kt algorithm versus the small-cone ones in the FIP algorithm.

Starting from these premises, and after reviewing in section 2 the theoretical setup for the description of Mueller-Navelet jets in terms of the collinear and high-energy factoriza-

[1] Here *kt algorithm* denotes the whole class of clustering algorithms based on ref. [7], which may differ in the details of the recombination scheme and of the resolution variable, like the *anti-kt* and the *Cambrigde/Aachen* versions.

JHEP04(2015)071

tion formulae, in section 3 we discuss in detail the differences among the three (kt, cone and FIP) jet algorithms in the relevant case of two near particles and we determine the kinematical configurations in the limit of small jet "radius" R.

We then derive the small-cone jet vertices for the kt and cone algorithms in section 4, by computing their differences with respect to the FIP algorithm induced by the different kinematical conditions.

In section 5 we perform a numerical study in order to asses the quantitative difference between the exact and small-cone jet vertex in the kt algorithm, by comparing the vertices themselves as well as a typical differential cross section for MN jets and some angular coefficients measuring the azimuthal decorrelation between the jets. In addition we also determine the discrepancies of the same quantities induced by a different choice of the jet algorithm.

We discuss the results in section 6, where we conclude that the wrong choice of algorithm causes sizeable errors on the predictions, while the SCA within the same algorithm provides a good approximation to the exact quantities and can therefore be used as a valuable tool for a quantitative description of MN and forward jets.

2 Theoretical setup

2.1 Factorization

The process we are considering was suggested long ago by Mueller and Navelet [1] in order to study the high-energy behaviour of QCD. It is generated by the collision of two hadrons $H_{A,B}$ — typically (anti)protons — and is characterized by the detection in the final state of two hard jets $J_{1,2}$ with large rapidity separation:

$$H_A + H_B \to J_1 + J_2 + X \tag{2.1}$$

where X represents any additional emission. Each jet J_i represents a cluster of particles grouped together according to some given jet algorithm and is described by 3 variables: the rapidity y_i, the *transverse* energy $E_i \equiv |\boldsymbol{k}_{J,i}|$ and the azimuthal angle $\phi_i \equiv \arg(\boldsymbol{k}_{J,i})$, $\boldsymbol{k}_{J,i}$ being the i-th jet transverse momentum.

The kinematical region where one expects the high-energy QCD dynamics to play an important role is given by

$$s \equiv (p_A + p_B)^2 \gg E_1^2 \sim E_2^2 \gg \Lambda^2_{\mathrm{QCD}} \,, \qquad |Y| \equiv |y_1 - y_2| \gg 1 \,, \tag{2.2}$$

where the condition of hard jets ($E_i^2 \gg \Lambda^2_{\mathrm{QCD}}$) is imposed for the applicability of perturbation theory.

In the leading twist approximation, i.e., up to power suppressed correction in the hard scale parameter $\Lambda^2_{\mathrm{QCD}}/E^2 \ll 1$, the hadronic cross section σ can be factorized in the (longitudinal momentum fraction) convolution of two partonic distribution functions (PDFs) $f_{a/H}(x)$ and a partonic cross section $\hat{\sigma}$

$$\frac{\mathrm{d}\sigma_{AB}(s)}{\mathrm{d}J_1 \mathrm{d}J_2} = \sum_{a,b} \int_0^1 \mathrm{d}x_1 \mathrm{d}x_2 \; f_{a/A}(x_1) f_{b/B}(x_2) \frac{\mathrm{d}\hat{\sigma}_{ab}(x_1 x_2 s)}{\mathrm{d}J_1 \, \mathrm{d}J_2} \,, \qquad \mathrm{d}J_i \equiv \mathrm{d}y_i \, \mathrm{d}E_i \, \mathrm{d}\phi_i \,, \tag{2.3}$$

JHEP04(2015)071

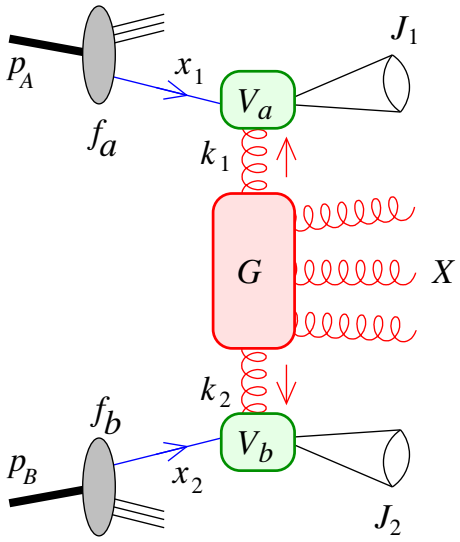

Figure 1. Diagrammatic representation of the collinear and high-energy factorization formula for Mueller-Navelet jet production: $f_{a,b}$ represents the parton densities, $V_{a,b}$ the jet vertices and G the gluon Green's function.

where $a, b \in \{q, g\}$ denote the parton flavours (quark or gluon) and x_i the partonic momentum fractions w.r.t. their parent hadrons. In turn, in the high-energy Regge regime we are considering, the partonic cross section for jet production can be factorized in a (transverse momentum) convolution of (process dependent) jet vertices V and a universal factor G called gluon Green's function (GGF)

$$\frac{\mathrm{d}\hat{\sigma}_{ab}(x_1 x_2 s)}{\mathrm{d}J_1\,\mathrm{d}J_2} = \int \mathrm{d}^2\boldsymbol{k}_1\,\mathrm{d}^2\boldsymbol{k}_2\; V_a(x_1, \boldsymbol{k}_1; J_1) G(x_1 x_2 s, \boldsymbol{k}_1, \boldsymbol{k}_2) V_b(x_2, \boldsymbol{k}_2; J_2)\;, \tag{2.4}$$

where $\boldsymbol{k}_i$ denotes the (reggeized) gluon transverse momentum flowing out from the GGF and entering the jet vertex, while $\hat{s} \equiv x_1 x_2 s$ is the center-of-mass energy squared of the partonic subsystem. The overall factorization structure is depicted in figure 1.

The PDFs are non-perturbative objects that depend also on the renormalization and factorization scales μ_R, μ_F. While μ_R is introduced in the renormalization of UV divergencies, μ_F enters in the treatment of the IR collinear divergencies which are absorbed by the PDFs. The μ_F dependence of the PDFs is governed by the DGLAP equations [16–18], and their evolution kernels (splitting functions) are known at next-to-next-to-leading order (NNLO). By means of global fits they have been determined in a wide range of the (x, μ_F^2) plane.

The GGF is the central object in high-energy QCD, in that it resums the $\log(s)$ to all orders in perturbation theory. It obeys the BFKL equation [19–22]

$$\omega G_\omega(\boldsymbol{k}_1, \boldsymbol{k}_2) = \delta^2(\boldsymbol{k}_1 + \boldsymbol{k}_2) + \int \mathrm{d}^2\boldsymbol{k}\; K(\boldsymbol{k}_1, \boldsymbol{k}) G_\omega(\boldsymbol{k}, \boldsymbol{k}_2) \tag{2.5}$$

$$G(\hat{s}, \boldsymbol{k}_1, \boldsymbol{k}_2) = \int_{-\mathrm{i}\infty}^{\mathrm{i}\infty} \frac{\mathrm{d}\omega}{2\pi\mathrm{i}} \left(\frac{\hat{s}}{s_0}\right)^\omega G_\omega(\boldsymbol{k}_1, \boldsymbol{k}_2)\;, \tag{2.6}$$

JHEP04(2015)071

where G_ω is the Mellin transform of $G(\hat{s})$, defined in terms of an arbitrary energy scale s_0. The BFKL kernel $K = \alpha_s K^{(0)} + \alpha_s^2 K^{(1)}$ is known in next-to-leading-logarithmic (NLL) approximation. The coefficient $K^{(1)}$ depends on the choice of both μ_R and s_0.

Finally, the jet vertices are perturbative finite objects without energy ($\sqrt{s}$) dependence, and are known in NLO approximation: $V = \alpha_s V^{(0)} + \alpha_s^2 V^{(1)}$. They depend on the jet variables y, E, ϕ and also on the arbitrary scales μ_R, μ_F, s_0, in such a way that the hadronic cross section be independent of those scales up to NLL terms, i.e., the scale dependence is present only in the terms of relative order $\alpha_s^2(\alpha_s \log(s))^n$.

It is apparent that the determination of the Mueller-Navelet (MN) jet cross section involves quite a number of integrals, both in the factorization formulae (2.3), (2.4), and in the determination of G and V, as can be checked from their explicit expressions [4, 5]. Furthermore, when comparing the theoretical predictions with experiments, one needs integrated cross sections in some of the jet variables, in order to comply with the experimental binning. Such integrations are mostly done numerically, and this would require a large amount of computing resources or time for reaching a precision at the level of 1%.

In order to cope with such a problem, two techniques can be exploited so as to reduce the computing time and improve convergence:

- to project the GGF and jet vertices on a complete set of functions which respects the symmetries of the process (e.g., azimuthal invariance);
- to use an approximated and simpler version of the jet vertices.

These methods are often used in BFKL phenomenological analyses, and we shall illustrate them in the following subsections: the former in order to set up the theoretical framework and the main notations; the latter in order to introduce the main subject of this paper.

2.2 Representation in Mellin space

The first method to reduce computing time does not involve any approximation, at least at the NLL level of accuracy we are working with. It is better illustrated in the LL approximation, where the strong coupling α_s is fixed and thus the BFKL kernel and jet vertices, in addition of being invariant under azimuthal rotations, are also scale invariant.[2] In this case, a Fourier-Mellin transform diagonalizes the transverse integrations and the ensuing expressions are considerably simpler to evaluate.

One can proceed in this way: first of all, let's exploit the fact that, in the LL approximation, each partonic momentum fraction coincides with the corresponding jet's longitudinal momentum fraction (because of a $\delta(x - x_J)$ in $V^{(0)}$):

$$x = x_J \equiv E\mathrm{e}^{\pm y}/\sqrt{s} \qquad (+, - \text{ for jet } 1, 2)\,, \tag{2.7}$$

so that $\hat{s} = x_1 x_2 s = \mathrm{e}^Y E_1 E_2$, where $Y \equiv |y_1 - y_2|$ is the rapidity distance between the jets. If we adopt the convenient and natural choice of $s_0 = E_1 E_2$ as energy scale, the Green's

[2] Strictly speaking, in our notations they are homogeneous functions of the transverse momenta $\boldsymbol{k}$, $\boldsymbol{k}_J$.

JHEP04(2015)071

function (2.6) is now independent of the partonic momentum fractions:

$$G(\hat{s}, \boldsymbol{k}_1, \boldsymbol{k}_2) = \int_{-\mathrm{i}\infty}^{\mathrm{i}\infty} \frac{\mathrm{d}\omega}{2\pi\mathrm{i}}\, \mathrm{e}^{\omega Y} G_\omega(\boldsymbol{k}_1, \boldsymbol{k}_2) \equiv G(Y, \boldsymbol{k}_1, \boldsymbol{k}_2)\,, \qquad (s_0 = E_1 E_2) \tag{2.8}$$

Secondly, we introduce the *impact factor* by integrating a jet vertex with the corresponding parton density:

$$\Phi_A(\boldsymbol{k}; J) \equiv \sum_a \int_0^1 \mathrm{d}x\; f_{a/A}(x) V_a(x, \boldsymbol{k}; J)\,. \tag{2.9}$$

so that we can rewrite the factorization formula in the form

$$\frac{\mathrm{d}\sigma_{AB}}{\mathrm{d}J_1\,\mathrm{d}J_2} = \int \mathrm{d}^2\boldsymbol{k}_1\,\mathrm{d}^2\boldsymbol{k}_2\; \Phi_A(\boldsymbol{k}_1) G(Y, \boldsymbol{k}_1, \boldsymbol{k}_2) \Phi_B(\boldsymbol{k}_2)\,. \tag{2.10}$$

At this point we project kernel and vertices onto the eigenfunctions of the LL BFKL kernel

$$\mathcal{E}_{n\nu}(\boldsymbol{k}) \equiv \frac{1}{\sqrt{2}\pi} |\boldsymbol{k}^2|^{\mathrm{i}\nu - \frac{1}{2}} \mathrm{e}^{\mathrm{i}n\phi}\,, \qquad (n \in \mathbb{Z},\ \nu \in \mathbb{R})\,, \tag{2.11}$$

satisfying the completeness relation

$$\sum_{n\in\mathbb{Z}} \int_{-\infty}^{\infty} \mathrm{d}\nu\; \mathcal{E}_{n\nu}(\boldsymbol{k}) \mathcal{E}^*_{n\nu}(\boldsymbol{k}') = \delta^2(\boldsymbol{k} - \boldsymbol{k}') \tag{2.12}$$

and providing the LL eigenvalue function $\chi^{(0)}_{n\nu}$

$$[K^{(0)} \mathcal{E}_{n\nu}](\boldsymbol{k}) \equiv \int \mathrm{d}^2\boldsymbol{k}'\; K^{(0)}(\boldsymbol{k}, \boldsymbol{k}') \mathcal{E}_{n\nu}(\boldsymbol{k}') = \chi^{(0)}_{n\nu} \mathcal{E}_{n\nu}(\boldsymbol{k}) \tag{2.13}$$

$$\chi^{(0)}_{n\nu} = 2\psi(1) - \psi\left(\frac{1+n}{2} + \mathrm{i}\nu\right) - \psi\left(\frac{1+n}{2} - \mathrm{i}\nu\right)\,. \tag{2.14}$$

Finally, by inserting a completeness (2.12) between each pair of factors in (2.10), we arrive at the convenient expression for the differential cross section

$$\frac{\mathrm{d}\sigma_{AB}}{\mathrm{d}J_1\,\mathrm{d}J_2} = \sum_n (-1)^n \int \mathrm{d}\nu\; \Phi_{A\,n\nu}\, G_{n\nu}(Y)\, \Phi^*_{B\,n\nu}\,, \tag{2.15}$$

where in the last equality we have used the Fourier-Mellin transforms

$$\int \mathrm{d}^2\boldsymbol{k}\; \Phi(\boldsymbol{k}; J) \mathcal{E}_{n\nu}(\boldsymbol{k}) \equiv \Phi_{n\nu}(J) \tag{2.16}$$

$$\int \mathrm{d}^2\boldsymbol{k}\,\mathrm{d}^2\boldsymbol{k}'\; \mathcal{E}^*_{n\nu}(\boldsymbol{k}) G(Y, \boldsymbol{k}, \boldsymbol{k}') \mathcal{E}_{n'\nu'}(\boldsymbol{k}') \equiv G_{n\nu}(Y) (-1)^n \delta_{nn'} \delta(\nu - \nu')\,. \tag{2.17}$$

The delta functions on the r.h.s. of eq. (2.17) are just a consequence of the azimuthal- and scale-invariance of the kernel, and allow us to trade two bidimensional integrals for a sum and a simple integral.

The azimuthal correlation of the MN jets is usually measured by means of the Fourier coefficients ($m \in \mathbb{Z}$)

$$C_m(E_1, y_1; E_2, y_2) \equiv \int_0^{2\pi} \mathrm{d}\phi_1 \mathrm{d}\phi_2\; \cos\big(m(\phi_1 - \phi_2 - \pi)\big) \frac{\mathrm{d}\sigma}{\mathrm{d}J_1\,\mathrm{d}J_2}\,. \tag{2.18}$$

JHEP04(2015)071

Because of the azimuthal- and scale-invariance of the vertices, it is easy to show that

$$\Phi_{n\nu}(y, E, \phi) = \mathrm{e}^{\mathrm{i}n\phi}(E^2)^{\mathrm{i}\nu-1}\Psi_{n\nu}(x_J) \;, \qquad \Psi_{n\nu} = \Psi_{-n\nu} \tag{2.19}$$

where Ψ is dimensionless,[3] thus obtaining a factorization formula with just one integration:

$$C_m = \left(\frac{2\pi}{E_1 E_2}\right)^2 \int \mathrm{d}\nu \left(\frac{E_1^2}{E_2^2}\right)^{\mathrm{i}\nu} \Psi_{A\,m\nu}\, G_{m\nu}(Y)\, \Psi^*_{B\,m\nu} \;. \tag{2.20}$$

Such a structure is preserved in the NLL approximation too, provided the impact factors and GGF are suitably modified in order to take into account the loss of scale-invariance due to the renormalization procedure and to the factorization of collinear singularities, which translates in a dependence on $\log(E/\mu_R)$, $\log(E/\mu_F)$ and $\log(E/\sqrt{s_0})$ of the GGF and impact factors. The expression of the GGF in Mellin-space is very simply expressed in terms of the eigenvalue $\chi_{n\nu}$ of the BFKL kernel:

$$G_{n\nu}(Y) = \mathrm{e}^{Y\chi_{n\nu}} \;, \qquad \chi_{n\nu} = \bar{\alpha}_s\chi^{(0)}_{n\nu} + \bar{\alpha}_s^2\chi^{(1)}_{n\nu} \tag{2.21}$$

However, the computation of $\Psi_{n\nu}$ at NLL level involves several integrations. The main advantage of this procedure is that such integrations can be done once and for all for each set of one-jet variables. Nevertheless, such computations can still be rather lengthy, and the use of an approximate expression of the impact factors — to be described in the next subsection — turns out to be very convenient.

Let us conclude this section by noticing that the factorization formula (2.20) is very useful also in the case of cross-section integrated in jet energies. In fact, a double integral in E_1 and E_2 factorizes into the product of simple integrals of the impact factors (provided the integration domain $D = I_1 \times I_2$ can be factorized into the cartesian product of two one-dimensional sets)

$$\begin{aligned} \boldsymbol{C}_m(y_1, y_2) &\equiv \int_{D=I_1\times I_2} \mathrm{d}E_1\mathrm{d}E_2\; C_m \\ &= (2\pi)^2 \int \mathrm{d}\nu\; G_{m\nu}(Y) \left[\int_{I_1} \mathrm{d}E_1\; (E_1^2)^{\mathrm{i}\nu-1}\Psi_{A\,m\nu}\right] \left[\int_{I_2} \mathrm{d}E_2\; (E_2^2)^{\mathrm{i}\nu-1}\Psi_{B\,m\nu}\right]^* \\ &\equiv (2\pi)^2 \int \mathrm{d}\nu\; G_{m\nu}(Y)\; \boldsymbol{\Psi}_{A\,m\nu}(y_1)\; \boldsymbol{\Psi}^*_{B\,m\nu}(y_2) \;. \end{aligned} \tag{2.22}$$

In this case, the integrated impact factors $\boldsymbol{\Psi}$ can be computed independently and stored in suitable grids, thus reducing a lot the computational effort of the phase-space integration. In the general case $D \neq I_1 \times I_2$, however, the expression (2.20) has to be numerically integrated in energy (and possibly in rapidity), and a suitable approximation (like the SCA) could be a very valuable tool to diminish the computing demand.

2.3 Small-cone approximation

In order to study the behaviour of the jet vertex for small values of the "radius" R — to be precisely defined later on — and possibly to speed up the computation of the jet

[3] We shall sometimes refer to the reduced impact factor Ψ as jet vertex.

JHEP04(2015)071

impact factor $\Psi_{n\nu}$ and of its energy-integrated version $\mathbf{\Psi}_{n\nu}$, one can use the small-cone approximation (SCA), as suggested and derived in [6]. The dependence of the impact factor on the jet radius R has the form [10, 11] (μ is a shorthand for μ_R, μ_R and $\sqrt{s_0}$)

$$\Psi_{n\nu}\Big(x_J, \log\frac{E}{\mu}; R\Big) = A_\nu(x_J)\log(R) + B_{n\nu}\Big(x_J, \log\frac{E}{\mu}\Big) + \mathcal{O}\left(R^2\right) \tag{2.23}$$

and the analytic expressions for the coefficients A, B were explicitly computed [6] for a particular jet algorithm (FIP).

However, whereas the coefficient A of $\log(R)$ depends only on the incoming hadron and is given in terms of the usual splitting functions as

$$A_\nu = -\alpha_s^2 \frac{\sqrt{N_c^2-1}}{\sqrt{2}\pi^2 N_c} x_J \int_{x_J}^1 \mathrm{d}\zeta\, \zeta^{-2\mathrm{i}\nu} \Bigg\{ \big[P_{qq}(\zeta) + P_{gq}(\zeta)\big] \sum_{a\in\{q,\bar{q}\}} f_a\Big(\frac{x_J}{\zeta}\Big) \tag{2.24}$$

$$+ \big[P_{gg}(\zeta) + 2n_f P_{qg}(\zeta)\big] f_g\Big(\frac{x_J}{\zeta}\Big)\Bigg\}\,, \tag{2.25}$$

the constant term B depends also on the details of the jet algorithm. Ivanov and Papa [6] computed such coefficient for an algorithm which was used in pioneering work on QCD jets by Furman [9] — we shall refer to it as FIP algorithm — which, however, is no more used in present day phenomenology.

The main purpose of our paper is to derive such coefficient for the two mostly used algorithms of QCD analysis, namely the cone-algorithm and the kt-algorithm. The computations can be repeated by following the procedure of [6].

The expressions for the jet vertices at LL and NLL level are extracted from the perturbative calculation of processes with two incoming partons producing 2-jet at LO and NLO respectively. At LO the amplitudes have just two partons in the final states, each of which is identified with a jet. The jets are emitted back-to-back in the azimuthal direction and have no substructure. Therefore no dependence on the algorithm is found at LO.

The same is true at NLO as far as the virtual corrections are concerned. On the other hand, the NLO real corrections involve 3 partons in the final state, therefore a jet can be constituted by either one or two of them. In the case of 1-parton (simple) jet, all algorithms are designed in such a way that no further emission is found within a region of radius R in the (y, ϕ) plane around the position of that parton.

Therefore, the differences among the algorithms are to be found in the 2-parton (composite) jet configurations. In the following section we will carefully compare the definitions the *cone*, *kt*, and *FIP* jet algorithms and, from their differences, we shall compute the small-cone impact factors for the cone and kt jets.

3 Jet algorithms

3.1 The cone algorithm

According to ref. [8], when two partons p_1 and p_2 are combined into one jet of radius R, the resulting jet variables (y, E, ϕ) are defined to be

$$E = E_1 + E_2\,, \qquad y = \frac{y_1E_1 + y_2E_2}{E}\,, \qquad \phi = \frac{\phi_1E_1 + \phi_2E_2}{E}\,. \tag{3.1}$$

JHEP04(2015)071

To determine whether the two partons are to be combined, we see if they fit in a cone of radius R about the jet axis in the (y, ϕ) plane. In practice, by denoting with Ω_{ij} the (y, ϕ)-distance

$$\Omega_{ij}^2 \equiv (y_i - y_j)^2 + (\phi_i - \phi_j)^2 \tag{3.2}$$

one requires $\Omega_{1J} < R$ and $\Omega_{2J} < R$ for the composite jet, which amounts the condition

$$\Omega_{12} < R \frac{E_1 + E_2}{\max(E_1, E_2)} \,. \tag{3.3}$$

A simple jet can then be defined only if the two partons cannot be combined, i.e., provided

$$\Omega_{12} > R \frac{E_1 + E_2}{\max(E_1, E_2)} \,. \tag{3.4}$$

3.2 The kt algorithm

According to ref. [7], the kt clustering algoritm consists in an iterative procedure which is based on comparing a set of resolution variables of single-particle d_{iB} (B for beam) and pairs d_{ij}

$$d_{iB} \equiv E_i^2 \,, \qquad d_{ij} \equiv \min(E_i^2, E_j^2) \, \frac{\Omega_{ij}^2}{R^2} \,. \tag{3.5}$$

One then considers the smallest one: if it is a d_{iB}, particle i is thrown in the beam basket and removed from the list; if it is a d_{ij} then particles i and j are merged into a pseudoparticle $\{ij\}$ — e.g., by using the recombination scheme (3.1). The procedure is repeated from the beginning, until all resolution variables are greater than some (hard) stopping parameter $d_{\rm cut} \gg \Lambda_{\rm QCD}^2$.

In the case of three partons in the final state there are these possibilities:

- One of the d_{iB}, say d_{1B} is the smallest resolution variable.
  - If $d_{1B} < d_{\rm cut}$ then particle 1 belongs to the beam and we are left with two partons which, if not in the beam, form two simple jets;
  - If $d_{1B} > d_{\rm cut}$ then the clustering stops and all three particles form simple jets;
- One of the d_{ij}, say d_{12} is the smallest resolution variable. In this case 1 and 2 are merged into a pseudoparticle $\{12\}$ and one considers three resolution variables: $d_{\{12\}B}$, d_{3B} and $d_{\{12\}3}$.
  - If the smallest is larger than $d_{\rm cut}$ clustering stops and we have one simple jet $\{3\}$ and one composite jet $\{12\}$;
  - If the smallest is less than $d_{\rm cut}$, a (pseudo)particle belongs to the beam and we cannot have two jets in the final state;

To summarize, we have a composite jet, say $\{12\}$, only if

$$d_{12} < d_{iB} \; \forall i \qquad \Longrightarrow \qquad \Omega_{12} < R \,. \tag{3.6}$$

In the other case

$$\Omega_{12} > R \tag{3.7}$$

only simple jets are present.

3.3 The Furman algorithm

In [6] Ivanov and Papa define a jet as a set of particles within a cone of radius R. To be more precise, they require that:

- the jet's momentum is the sum of the particles' momenta;
- all and only the particles of the jet belong to a circle of radius R in the (y, ϕ) plane and centered at the jet's momentum.

This is just the jet definition of Furman [9] used in the '80s for early phenomenology of NLO QCD jets — we denote it "FIP algorithm".

In the case under study, where at most two particles (1 and 2) can form a jet, the condition for a composite jet is nothing but the prescription adopted in the cone algorithm: two particles such that

$$\Omega_{12} < R\frac{E_1 + E_2}{\max(E_1, E_2)} \tag{3.8}$$

can be considered as a composite jet. On the other hand, particle 1 can form a simple jet if no other particle is found within a distance R from it, namely

$$\Omega_{12} > R\,. \tag{3.9}$$

This definition is somewhat pathological, because it may happen that a given configuration can give rise to both a composite jet and two simple jets. This fact can be easily understood in the case of two particles with the same transverse energy and whose distance satisfy $R < \Omega_{12} < 2R$. They can form simple jets because a cone of radius R centered on either particle does not contain the other; on the other hand, a cone of radius R centered halfway the two particles contains both of them. For this reason, it is not possible to extend such jet definition into an IR-safe algorithm to all orders, i.e., with an arbitrary number of particles, hence it has been abandoned in favour of better algorithms like the cone and especially the kt one.

In any respect, this definition is different from both the cone algorithm (in the case of simple jets) and the kt algorithm (in the case of composite jets), and yields different results when used to defined any observable. It is the main purpose of this paper to derive the correct expressions for the jet vertices in the SCA for the kt algorithm and also for the cone one.

4 Small cone jet vertices

In this section we shall compute the SCA jet vertex in the cone and kt algoritm. The idea is to identify and calculate the contributions differing from those of the original paper [6] where the FIP algorithm was adopted.

As explained in the previous section, for dijet production at NLO, the differences among jet algorithms occur only in the way that two partons can be combined to form a jet. In the BFKL approach, two partons (1 and 2) in the fragmentation region of an

JHEP04(2015)071

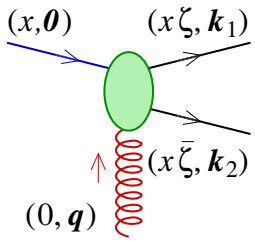

Figure 2. Kinematics of the fragmentation region of hadron A: the collision of the incoming parton (blue) and of the Regge gluon (red) produces a pair of outgoing partons (black). In parentheses the longitudinal momentum fraction and the transverse momentum of each particle.

incoming hadron are produced by the interaction of a parton stemming from the hadron and a reggeized gluon, as depicted in figure 2.

In the high-energy kinematics, the incoming parton has just a fraction x of the pure longitudinal momentum of the hadron, while the reggeized gluon's momentum q is essentially transverse. Following Ivanov-Papa (IP) [6] we work in dimensional regularization ($D = 4 + 2\epsilon$) and we indicate with k_1 (k_2) the $(2 + 2\epsilon)$-dimensional transverse momentum of the outgoing parton 1 (2), and with ζ ($\bar{\zeta} \equiv 1 - \zeta$) its longitudinal momentum fraction with respect to the incoming parton. In terms of these variables, the relative rapidity and azimuthal angle between the two outgoing partons are

$$\Delta y = \frac{1}{2} \log \frac{\zeta^2 k_2^2}{\bar{\zeta}^2 k_1^2} , \qquad \Delta\phi = \arccos \frac{k_1 \cdot k_2}{|k_1|\,|k_2|} , \qquad \bar{\zeta} \equiv 1 - \zeta . \tag{4.1}$$

We shall present our results by using the notations of ref. [6], namely in term of their "I" quantities, which are related to our definition of jet impact factor (2.16) by

$$\Phi_{n\nu}(y, E, \phi) = \alpha_s \frac{\sqrt{N_c^2 - 1}}{\sqrt{2}\pi N_c} \frac{x_J}{E}\, I(n, \nu; y, E, \phi) , \qquad I = \sum_{i,f} (I^R_{i;f} + I^V_{i;f}) , \tag{4.2}$$

where i (f) are labels for the initial (final) state of the sub-processes contributing to the cross section, while the superscripts R and V denote real and virtual parts respectively.

4.1 Vertex for the cone algorithm

The condition for composite jet in the cone algorithm (3.3) coincides with the one adopted by FIP (3.8), thus no difference is expected for the corresponding contributions.

In contrast, the conditions for simple jets (3.4) and (3.9) are different, causing different contributions to the jet vertices. By using the notations of ref. [6], $k = k_1$ is the transverse momentum of the parton forming the simple jet, $q - k = k_2$ is the transverse momentum of the parton outside the jet (also called "spectator"), and one introduces the transverse vector $\boldsymbol{\Delta}$

$$q = \frac{k}{\zeta} + \boldsymbol{\Delta} \tag{4.3}$$

which vanishes when the two partons are collinear. In fact, for small $\boldsymbol{\Delta}$, we have

$$\Omega_{12}^2 \equiv \Delta\phi_{12}^2 + \Delta y_{12}^2 \simeq \frac{\zeta^2}{\bar{\zeta}^2} \frac{\boldsymbol{\Delta}^2}{k^2} \tag{4.4}$$

JHEP04(2015)071

and also

$$\frac{E_1+E_2}{\max(E_1,E_2)}=\frac{|k_1|+|k_2|}{\max(|k_1|,|k_2|)}\simeq\frac{|k|\left(1+\frac{\bar\zeta}{\zeta}\right)}{|k|\max\left(1,\frac{\bar\zeta}{\zeta}\right)}=\frac{1}{\max(\zeta,\bar\zeta)} \tag{4.5}$$

Therefore, the simple-jet condition (3.3) becomes

$$|\mathbf{\Delta}|>\frac{\bar\zeta}{\zeta}|k|\frac{R}{\max(\zeta,\bar\zeta)}\,, \tag{4.6}$$

at variance with the FIP condition (3.8) which, expressed in terms of $\mathbf{\Delta}$, reads like eq. (4.6) but without the denominator $\max(\zeta,\bar\zeta)$ [6].

In order to identify the contributions of the FIP jet vertex that have to be modified in the cone algorithm, let us recall that the simple jet configurations were computed in two steps: *1)* by allowing the spectator parton to span the whole phase space and then *2)* by subtracting the contribution stemming from the spectator parton inside the jet cone. Therefore, we have to modify only the subtractions by replacing $R\to R/\max(\zeta,\bar\zeta)$.

The *quark initiated* jet vertex (quark+Regge-gluon → quark+gluon, see figure 2) has two such subtractions, one for the quark-jet and one for the gluon-jet, whose results are reported in eqs. (5.36) and (5.38) of ref. [6] respectively. In the gluon-jet term the substitution $R\to R/\max(\zeta,\bar\zeta)$ is straightforward:

$$\begin{aligned}I^R_{q;g,-q}=(5.36)[1]\to&-\frac{\alpha_s}{2\pi}\frac{\Gamma(1-\epsilon)}{\epsilon(4\pi)^\epsilon}\frac{\Gamma^2(1+\epsilon)}{\Gamma(1+2\epsilon)}(k^2)^{\gamma+\epsilon-\frac{n}{2}}(k\cdot l)^n\int_{x_J}^1\frac{\mathrm{d}\zeta}{\zeta}\,\zeta^{-2\gamma}\sum_{a=q,\bar q}f_a\left(\frac{x_J}{\zeta}\right)\\&\times\left(\frac{R}{\max(\zeta,\bar\zeta)}\right)^{2\epsilon}\left[P_{gq}(\zeta)\left(1+2\epsilon\log\frac{\bar\zeta}{\zeta}\right)+\epsilon C_F\zeta\right]\\=I^R_{q;g,-q}-&\frac{\alpha_s}{2\pi}(k^2)^{\gamma-\frac{n}{2}}(k\cdot l)^n\int_{x_J}^1\frac{\mathrm{d}\zeta}{\zeta}\,\zeta^{-2\gamma}\sum_{a=q,\bar q}f_a\left(\frac{x_J}{\zeta}\right)P_{gq}(\zeta)2\log\left(\max(\zeta,\bar\zeta)\right)\,,\end{aligned} \tag{4.7}$$

where $\gamma\equiv\mathrm{i}\nu-\frac{1}{2}$ and $l\equiv e_1+\mathrm{i}e_2$ is a complex vector lying only in the first two of the $2+2\epsilon$ transverse dimensions.

In the quark-jet one has to proceed more carefully, because of the presence of a double pole in ϵ multiplying $(R/\max(\zeta,\bar\zeta))^\epsilon$. This would generate, among other things, modified simple poles and also finite double logs. However, since the double pole is multiplied by a $\delta(1-\zeta)$, for these terms $\max(\zeta,\bar\zeta)=1$ and the outcome is identical to the FIP algorithm. The only difference comes from the simple pole in front of the P_{qq} splitting function, and we obtain

$$\begin{aligned}I^R_{q;q,-g}=&\,(5.38)[1]\\\to&\,I^R_{q;q,-g}-\frac{\alpha_s}{2\pi}(k^2)^{\gamma-\frac{n}{2}}(k\cdot l)^n\int_{x_J}^1\frac{\mathrm{d}\zeta}{\zeta}\,\zeta^{-2\gamma}\sum_{a=q,\bar q}f_a\left(\frac{x_J}{\zeta}\right)P_{qq}(\zeta)2\log\left(\max(\zeta,\bar\zeta)\right)\,.\end{aligned} \tag{4.8}$$

The *gluon initiated* jet vertex has two subtractions too, one for the $q\bar q$ final state and one for the gg final state, whose results are reported in eqs. (5.49)[4] and (5.56) of

[4] We note a misprint in ref. [6]: in eqs. (5.48-49) the first subscript of I^R should be g instead of q. Also the last subscript in eq. (5.38) should be $-g$ instead of $-q$.

JHEP04(2015)071

ref. [6] respectively. The situation is very similar to that of the quark initiated vertex: the subtraction in the (anti)quark jet contains a simple pole times the $P_{qg}(\zeta)$ splitting function in front of the $R^{2\epsilon}$ factor, while the gluon jet contains both single and double poles, the former with the $P_{gg}(\zeta)$ splitting function and the latter with the $\delta(1-\zeta)$ distribution. For both types of jets the substitution $R \to R/\max(\zeta,\bar\zeta)$ simply amounts to finite contributions proportional to $\log\big(\max(\zeta,\bar\zeta)\big)$:

$$\begin{aligned} &I^R_{g;q,-\bar q} + I^R_{g;\bar q,-q} + I^R_{g;g,-g} = (5.49)[1] + \{q \leftrightarrow \bar q\} + (5.56)[1] \\ &\to I^R_{g;q,-\bar q} + I^R_{g;\bar q,-q} + I^R_{g;g,-g} \\ &\quad - \frac{\alpha_s}{2\pi}(k^2)^{\gamma-\frac{n}{2}}(k\cdot l)^n \int_{x_J}^1 \frac{\mathrm{d}\zeta}{\zeta}\,\zeta^{-2\gamma} \sum_{a=q,\bar q} f_a\left(\frac{x_J}{\zeta}\right)\left[2n_f P_{qg}(\zeta) + P_{gg}(\zeta)\right] 2\log\max(\zeta,\bar\zeta)\,. \end{aligned} \tag{4.9}$$

To sum up, the jet vertex for the cone algorithm in the small-cone approximation is obtained by replacing $R \to R/\max(\zeta,\bar\zeta)$ in the final formulae (5.39) and (5.57) of [6]. The complete expressions are written in eqs. (4.19), (4.20).

4.2 Vertex for the kt algorithm

The condition for simple jet in the kt algorithm (3.7) coincides with the one adopted by FIP (3.9), while the conditions for composite jet (3.6) and (3.8) are different. In the composite jet configuration the jet's transverse momentum is $k = k_1 + k_2 = q$ and it is convenient to define the auxiliary transverse vector $\boldsymbol{\Delta}$ as

$$k_1 = \zeta k + \boldsymbol{\Delta} \tag{4.10}$$

thus obtaining

$$\Omega_{12}^2 = \frac{\boldsymbol{\Delta}^2}{k^2\zeta^2\bar\zeta^2} \tag{4.11}$$

The composite jet condition (3.6) becomes

$$|\boldsymbol{\Delta}| < \zeta\bar\zeta|k|R\,, \tag{4.12}$$

at variance with the FIP condition (3.8) which reads [6] $|\boldsymbol{\Delta}| < \min(\zeta,\bar\zeta)|k|R$.

The corresponding contributions of [6], that have to be modified in order to recover the jet vertex in the kt algorithm, are found in section 5.1.1.c for the quark initiated vertex and sections 5.2.1.b and 5.2.2.b for the gluon initiated one. In all such cases the modification amounts to replace

$$|\Delta_{\max}| = \min(\zeta,\bar\zeta)|k|R \to \zeta\bar\zeta|k|R\,, \tag{4.13}$$

and finally to substitute $\min(\zeta,\bar\zeta) \to \zeta\bar\zeta$ in the ζ-integral with the relevant splitting function.

Explicitly, in the *quark-initiated* case, such integrals for the FIP and kt algoritms reads respectively

$$I^{R\,(\mathrm{FIP})}_{q;q+g} \propto \int_0^1 \mathrm{d}\zeta\,[\min(\zeta,\bar\zeta)]^{2\epsilon}\frac{1+\bar\zeta^2+\epsilon\zeta^2}{\zeta} = \frac{1}{\epsilon} - \frac{3}{2} + \left(\frac{7}{2} - \frac{\pi^2}{3} + 3\log 2\right)\epsilon \tag{4.14}$$

$$I^{R\,(\mathrm{kt})}_{q;q+g} \propto \int_0^1 \mathrm{d}\zeta \qquad (\zeta\bar\zeta)^{2\epsilon} \quad \frac{1+\bar\zeta^2+\epsilon\zeta^2}{\zeta} = \frac{1}{\epsilon} - \frac{3}{2} + \left(\frac{13}{2} - \frac{2\pi^2}{3}\right)\epsilon\,. \tag{4.15}$$

JHEP04(2015)071

Their difference $(3-\pi^2/3-3\log 2)\epsilon$, when multiplied by the overall $1/\epsilon$ pole, provides a finite contribution that has to be added to the IP result in order to obtain the proper expression for the kt algorithm:

$$I^R_{q;q+g} = (5.33)[1] \to I^R_{q;q+g} + \frac{\alpha_s}{2\pi}(k^2)^{\gamma-\frac{n}{2}}(k\cdot l)^n \sum_{a=q,\bar q} f_a(x_J) C_F \left(3-\frac{\pi^2}{3}-3\log 2\right). \quad (4.16)$$

In the *gluon-initiated* case the procedure is identical; here we have two contributions: one from the $q\bar q$ jet

$$I^R_{g;q+\bar q} = (5.47)[1] \to I^R_{g;q+\bar q} + \frac{\alpha_s}{2\pi}(k^2)^{\gamma-\frac{n}{2}}(k\cdot l)^n \frac{C_A}{C_F} f_g(x_J)\, 2n_f T_R \left(\frac{2}{3}\log 2 - \frac{23}{36}\right), \quad (4.17)$$

and one from the gg jet

$$I^R_{g;g+g} = (5.54)[1] \to I^R_{g;g+g} + \frac{\alpha_s}{2\pi}(k^2)^{\gamma-\frac{n}{2}}(k\cdot l)^n \frac{C_A}{C_F} f_g(x_J) C_A \left(\frac{131}{36}-\frac{\pi^2}{3}-\frac{11}{3}\log 2\right). \quad (4.18)$$

The integrals (4.14), (4.15) and the analogous ones for the gluon-initiated contributions, yielding eqs. (4.16)–(4.18), were already considered and computed [10, 11] in the first study of the relation between the kt and the cone algorithm — the latter sharing with FIP the condition of composite jet.

4.3 Final expressions of the jet vertices

The result of the jet vertex for the cone and kt algoritms is reported below, by adding to the original expressions of IP [6] the modifications computed in the previous subsections and here highlighted in boldface: $\langle\cdots\rangle_{\boldsymbol{C}}$ for the cone and $\langle\cdots\rangle_{\boldsymbol{K}}$ for the kt. The quark part is

$$\begin{aligned}
I_q = \frac{\alpha_s}{2\pi}(k^2)^\gamma e^{in\phi} \int_{x_J}^1 \frac{d\zeta}{\zeta} \sum_{a=q,\bar q} f_a\left(\frac{x_J}{\zeta}\right) \Bigg\{ & \left[P_{qq}(\zeta) + \frac{C_A}{C_F} P_{gq}(\zeta)\right] \log\frac{k^2}{\mu_F^2} + \\
& - 2\zeta^{-2\gamma}[P_{qq}(\zeta)+P_{gq}(\zeta)] \log \frac{R}{\langle \mathbf{\max(\zeta,\bar\zeta)}\rangle_{\boldsymbol{C}}} - \frac{\beta_0}{2}\log\frac{k^2}{\mu_R^2}\delta(1-\zeta) \\
& + C_A\delta(1-\zeta)\left\{\chi^{(0)}_{n\nu}\log\frac{s_0}{k^2} + \frac{85}{18} + \frac{\pi^2}{2} + \frac{1}{2}\left[\psi'\left(1+\gamma+\frac{n}{2}\right) - \psi'\left(\frac{n}{2}-\gamma\right) - \chi^{(0)\,2}_{n\nu}\right]\right\} \\
& + (1+\zeta^2)\Bigg\{ C_A\left[\frac{(1+\zeta^{-2\gamma})\chi^{(0)}_{n\nu}}{2(1-\zeta)_+} - \zeta^{-2\gamma}\left(\frac{\log(1-\zeta)}{1-\zeta}\right)_+\right] \\
& + \left(C_F - \frac{C_A}{2}\right)\left[\frac{\bar\zeta}{\zeta^2}I_2 - \frac{2\log\zeta}{\bar\zeta} + 2\left(\frac{\log(1-\zeta)}{1-\zeta}\right)_+\right]\Bigg\} \\
& + \delta(1-\zeta)\left[C_F\left(3\log 2 - \frac{\pi^2}{3} - \frac{9}{2} + \left\langle \mathbf{3 - \frac{\pi^2}{3} - 3\log 2}\right\rangle_{\boldsymbol{K}}\right) - \frac{10}{9}n_f T_R\right] \\
& + C_A\zeta + C_F\bar\zeta + \frac{1+\bar\zeta^2}{\zeta}\left[C_A\frac{\bar\zeta}{\zeta}I_1 + 2C_A\log\frac{\bar\zeta}{\zeta} + C_F\zeta^{-2\gamma}(\chi^{(0)}_{n\nu} - 2\log\bar\zeta)\right]\Bigg\},
\end{aligned} \quad (4.19)$$

JHEP04(2015)071

where $\gamma \equiv \mathrm{i}\nu - 1/2$, $\beta_0 \equiv (11C_A - 4n_f T_R)/3$, ψ is the digamma function, while the splitting functions $P_{ab}(\zeta)$ and the special functions $I_j(n,\gamma,\zeta)$ are reported in appendix A.

The gluon part is

$$
\begin{aligned}
I_g = \frac{\alpha_s}{2\pi}(k^2)^\gamma \mathrm{e}^{\mathrm{i}n\phi} \int_{x_J}^1 \frac{\mathrm{d}\zeta}{\zeta} f_g\left(\frac{x_J}{\zeta}\right) \frac{C_A}{C_F} \Bigg\{ & \left[P_{gg}(\zeta) + \frac{C_A}{C_F} 2n_F P_{qg}(\zeta)\right] \log\frac{k^2}{\mu_F^2} + \\
& - 2\zeta^{-2\gamma}[P_{gg}(\zeta) + 2n_f P_{qg}(\zeta)] \log\frac{R}{\left\langle \mathbf{max(\zeta,\bar{\zeta})} \right\rangle_{\boldsymbol{C}}} - \frac{\beta_0}{2}\log\frac{k^2}{4\mu_R^2}\delta(1-\zeta) \\
& + C_A\delta(1-\zeta)\left\{ \chi_{n\nu}^{(0)} \log\frac{s_0}{k^2} + \frac{1}{2}\left[\psi'\left(1+\gamma+\frac{n}{2}\right) - \psi'\left(\frac{n}{2}-\gamma\right) - \chi_{n\nu}^{(0)\,2}\right] \right. \\
& \qquad \left. + \frac{1}{12} + \frac{\pi^2}{6} + \left\langle \frac{\mathbf{131}}{\mathbf{36}} - \frac{\boldsymbol{\pi^2}}{\mathbf{3}} - \frac{\mathbf{11}}{\mathbf{3}}\mathbf{log\,2} \right\rangle_{\boldsymbol{K}} \right\} \\
& + 2C_A(1-\zeta^{-2\gamma})\left[\left(\frac{1}{\zeta} - 2 + \zeta\bar{\zeta}\right)\log\bar{\zeta} + \frac{\log(1-\zeta)}{1-\zeta}\right] \\
& + C_A\left[\frac{1}{\zeta} + \frac{1}{(1-\zeta)_+} - 2 + \zeta\bar{\zeta}\right]\left[(1+\zeta^{-2\gamma})\chi_{n\nu}^{(0)} - 2\log\zeta + \frac{\bar{\zeta}^2}{\zeta^2} I_2\right] \\
& + 2n_f T_R\left[2\frac{C_F}{C_A}\zeta\bar{\zeta} + (\zeta^2+\bar{\zeta}^2)\left(\frac{C_F}{C_A}\chi_{n\nu}^{(0)} + \frac{\bar{\zeta}}{\zeta} I_3\right)\right. \\
& \qquad \left. \left. + \delta(1-\zeta)\left(-\frac{1}{12} + \left\langle \frac{\mathbf{2}}{\mathbf{3}}\mathbf{log\,2} - \frac{\mathbf{23}}{\mathbf{36}} \right\rangle_{\boldsymbol{K}}\right)\right] \right\}. \qquad (4.20)
\end{aligned}
$$

It is apparent from the above expression that the $\log(R)$ coefficient A of the jet vertex is independent of the jet algorithm, while the constant coefficient B depends on it.

5 Numerical study

In this section we assess the quantitative difference among the jet vertices in the three algorithms (cone, kt, FIP) that we considered, and also the corresponding accuracy of their small-cone approximations (SCA). We shall use the term *exact* in the sense of "without SCA".

5.1 Jet vertices versus R

We start by evaluating the "exact" jet vertices in the three algorithms — we employ the numerical code used in ref. [23] — for various values of the jet radius R, and we compare them with their SCA. We expect the SCA to be better, the smaller the values of R, and increasing discrepancy with increasing R. On the other hand, the differences among different algorithms shouldn't vanish with R, according to our analysis.

This is actually the case, as can be seen in figure 3, where we plot the exact (points) and small-cone (lines) NLO part of the jet vertex versus R, in the three algorithms mentioned before (for a given choice of the parameters n, ν, E, y). The common slope of the lines represents the coefficient A of $\log(R)$, which is the same for the three algorithms, while the intercepts at $R = 1$ give the constant coefficients B, which clearly depend on the algorithm. A detailed study, carried out with several values of the parameters, shows that

JHEP04(2015)071

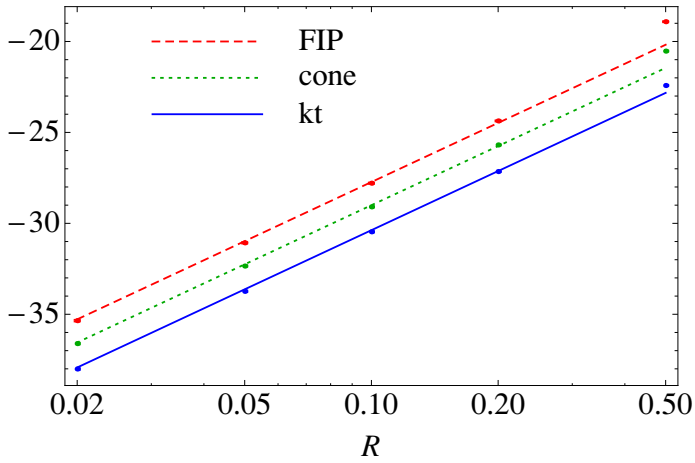

Figure 3. Dependence on the jet radius R of the NLO jet vertices Ψ in the three jet algorithms discussed in the text: FIP (dashed red), cone (dotted green) and kt (solid blue). The big dots correspond to the exact evaluation (the small error bars showing MonteCarlo integration uncertainties), while the straight lines denote the small-cone approximation. Here $n = 0$, $\nu = 0$, $y = 3.6$, $E = 35\,\mathrm{GeV}$.

the small-cone approximation works very well up to R of few tenths, with an error below 1% for $R \lesssim 0.2$ which increases up to 3–4% when $R = 0.5$.

5.2 SCA versus algorithm choice

Next, we specialize our analysis to realistic values of the jet radius and energy. Since the typical phenomenological studies on MN jets use $R \simeq 0.5$ and jet transverse energies $E \gtrsim 35\,\mathrm{GeV}$, in the following all quantities will be evaluated at $R = 0.5$ and $E = 35\,\mathrm{GeV}$. In addition, nowadays the mostly used jet algorithm is the kt. Therefore we adopt "exact" quantities, computed in the kt algorithm, as reference quantities, and we estimate the deviations to them introduced by the SCA.

To some extent, adopting the SCA at fixed R is a sort of choosing a jet algorithm. The natural question then arises: how does the discrepancy introduced by the small-cone approximation

$$\text{(exact-kt)} - \text{(SCA-kt)} \tag{5.1}$$

compare with the discrepancy caused by different choices of jet algorithm, i.e.,

$$\text{(SCA-kt)} - \text{(SCA-FIP)} \ ? \tag{5.2}$$

In order to answer this question, we compute the exact NLO part[5] of jet vertex $\Psi^{\mathrm{NLO}}_{n\nu}$ in the kt algorithm as function of ν, and compare it with the SCA in the same algorithm and also with the SCA in the FIP algorithm.

Figure 4 shows such a comparison for $n = 1$. We can see that the exact result in the kt algorithm is much better approximated by the SCA in the same algorithm rather than

[5]We recall that the LO part is independent of the jet algorithm.

JHEP04(2015)071

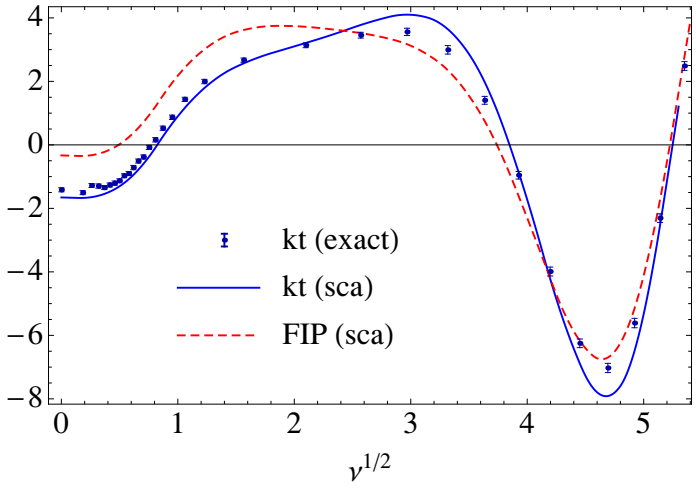

Figure 4. Comparison of the NLO exact jet vertex in the kt algorithm (points) with its SCA in the same algorithm (solid blue) and in the FIP algorithm (dashed red). Here $R = 0.5$, $n = 1$, $y = 3.6$, $E = 35\,\text{GeV}$.

by the FIP choice, in particular at small values of ν, which are the most important in the ν integrals of eqs. (2.20), (2.22) — since the GGF is peaked around $\nu = 0$.

This conclusion is further supported by analysing the whole (LO+NLO) ν-integrand of eq. (2.22), again by comparing exact-kt, SCA-kt and SCA-FIP, as in figure 5. The discrepancy introduced by the SCA in the wrong FIP algorithm is about three times larger than that introduced by the SCA in the proper kt algorithm, the latter being of the order of 5%.

Actually, the relative error due to the SCA is slightly larger for the full (LO+NLO) quantities than for the pure NLO ones. This is due to the fact that the NLO corrections usually have sign opposite to the common LO terms, giving rise to cancellations in their sum that amplify the relative differences.

5.3 Cross section and angular coefficients

Finally, we present the results of the differential cross section $\mathrm{d}\sigma/\mathrm{d}Y$ and of few angular coefficients C_m/C_n.

In figure 6 we plot the differential cross section $\mathrm{d}\sigma/\mathrm{d}Y = C_0(Y)$ by comparing again the exact kt calculation with the small-cone approximations in the KT and FIP algorithms.

It is evident that the wrong choice of the algorithm yields a large error, especially at lower values of Y, while the sole SCA with the proper algorithm introduces an error of 4–8%.

The shape of the C_0 curves, which are not monothonically decreasing in Y as one could naively expect, is due to an additional cut in rapidity $|y_i| > y_{\min} = 3$ that we have imposed just for computational convenience, as will be shortly explained. Due to this cut, the minimum value of Y that we allow is $Y_{\min} = 2y_{\min} = 6$ and in this limit the cross-section vanishes. It then quickly rises for $Y > 6$ before eventually decreasing at larger $Y \gtrsim 7$.

JHEP04(2015)071

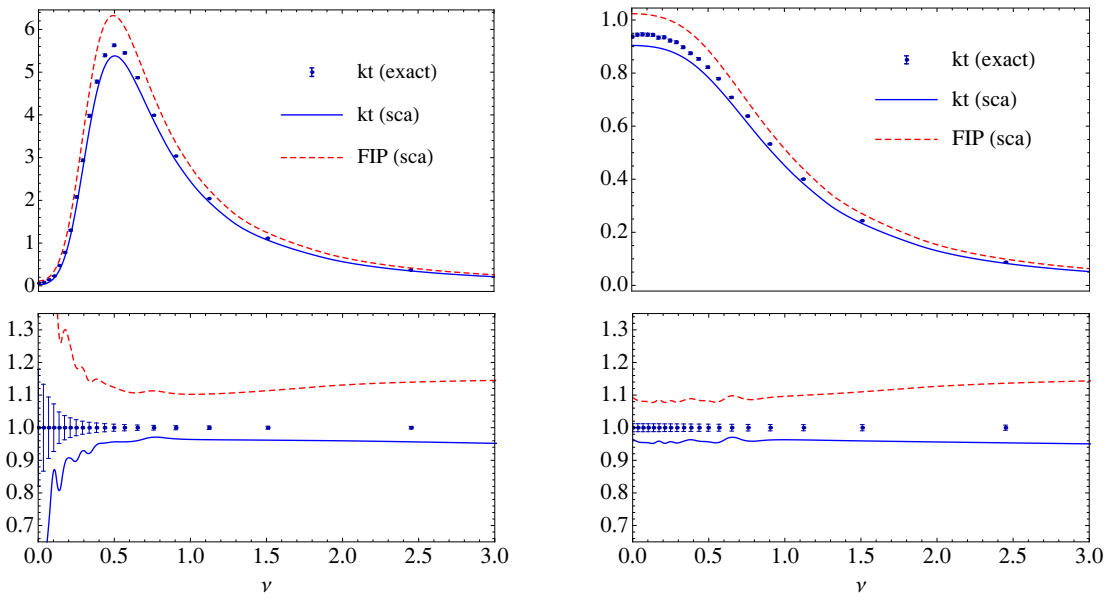

Figure 5. Comparison of the exact ν-integrand for kt algorithm (points) with the SCA in the same algorithm (solid blue) and in the FIP algorithm (dashed red). On the left: $n = 0$; on the right: $n = 1$. The upper plots display absolute values in arbitrary units, and below them we show the ratios w.r.t. exact integrand. The parameters are $R = 0.5$, $E_1 = E_2 = 35\,\mathrm{GeV}$, $y_1 = 3.6$, $y_2 = 2.8$.

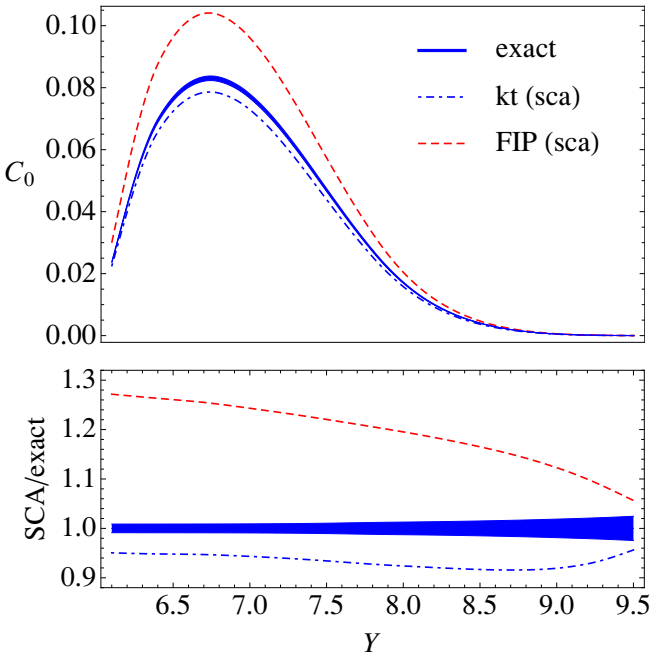

Figure 6. Comparison of the exact differential cross section $\mathrm{d}\sigma/\mathrm{d}Y$ ($n = 0$) for kt algorithm (solid blue) with the SCA in the same algorithm (dash-dotted blue) and in the FIP algorithm (dashed red). Top: absolute values in linear scale; bottom: ratios of the SCAs w.r.t. the exact one. Here $R = 0.5$, $E_1 = E_2 = 35\,\mathrm{GeV}$.

JHEP04(2015)071

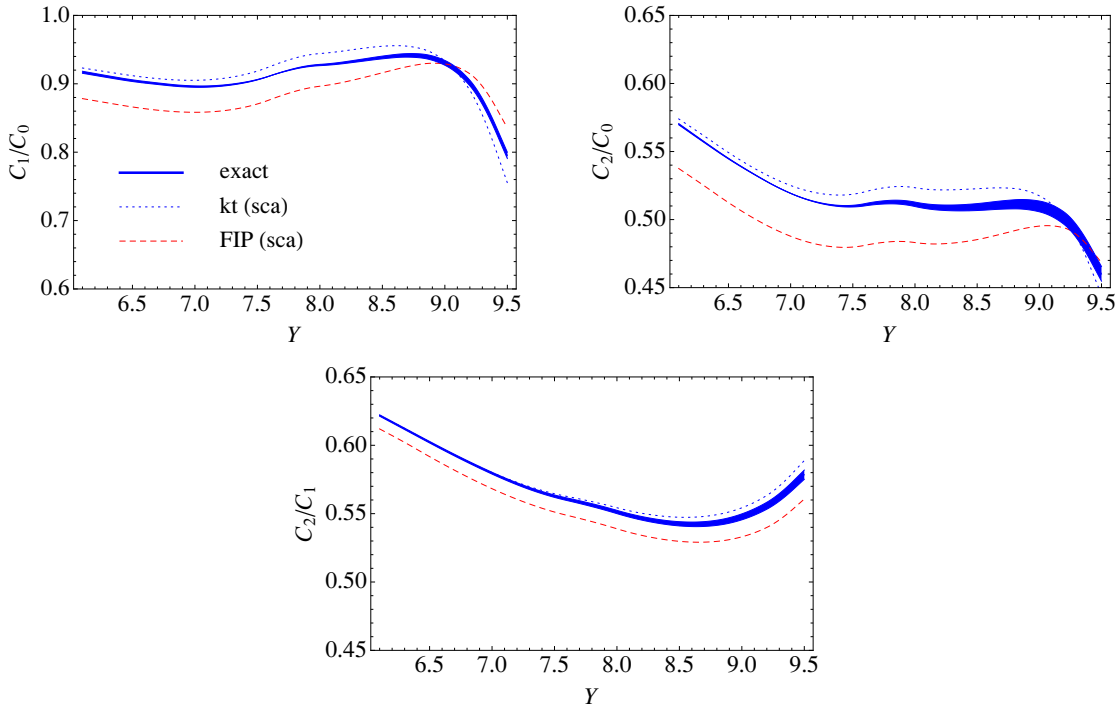

Figure 7. Comparison of some ratios C_m/C_n determined with the exact jet vertices in the kt algorithm (solid blue) with those obtained in the SCA with the same algorithm (dotted blue) and with the FIP algorithm (dashed red). Here $R = 0.5$, $E_1 = E_2 = 35$ GeV.

The reason for imposing the $|y_i| > y_{\min}$ cut is due to the fact that monochromatic (fixed E) impact factors oscillate at large ν, causing the ν integration in eq. (2.20) to be slowly convergent. Actually, the convergence is provided by the GGF, whose modulus decreases at large ν, the decrease being faster at larger values of Y. On the other hand, at low values of Y, and in particular with very asymmetric rapidity configurations ($\big||y_1| - |y_2|\big| \gg 1$), the numeric ν-integration has to be pushed to large ν-values, thus demanding a large computational effort. Since this problem is absent for realistic phenomenological studies (where the impact factors are integrated in the E variable and decrease themselves with ν), and because the goal of this analysis is just to compare the main features of the different algorithms, we solve the convergence issue by imposing the mentioned cut in rapidity $|y_i| > 3$.

From the plots of figures 5, 6 one can infer that the main effect of the SCA is mostly an overall normalization change, and that this is also true even for the wrong choice of algorithm (kt versus FIP), though with a larger factor. If this were the case, by computing *ratios* of observables such effects should cancel out and reproduce more faithfully the exact quantities. This is partially true, as can be seen in figure 7, where we plot some ratios of angular coefficients $C_m(Y)/C_n(Y) = \langle\cos(m\Delta\phi_J)\rangle/\langle\cos(n\Delta\phi_J)\rangle$ which are usually adopted in order to measure the azimuthal decorrelation of the MN jets.

It is nevertheless evident that the cancellation of the systematic effects is more effective if the SCA is made with the proper algorithm, leading to a discrepancy of about 2% or less for all the ratios considered. A different choice of algorithm yields definitely larger discrepancies, and therefore should be avoided.

JHEP04(2015)071

6 Conclusions

In this paper we have reconsidered the high-energy factorization formula for Mueller-Navelet jet production, and we have computed the NLO jet vertices in the small-cone approximation for two different jet algorithms: the *kt algorithm* and the *cone algorithm*.

The small-cone approximation amounts to evaluate the generic jet vertex Ψ at small jet radius $R \to 0$ according to the expansion $\Psi = A \log(R) + B + \mathcal{O}\left(R^2\right)$, where the coefficient A is universal, depending only on the infra-red properties of QCD, while the constant term B depends on the jet algorithm. It should be noted that the neglected term in the expansion is quadratic in R, and that the linear term is missing. It turns out that the small-cone approximation is quite accurate for realistic values of $R \lesssim 0.5$ and, because of its analytic and computational simplicity, it has been and will be used with benefit.

The calculation of the Mellin-Fourier components of the jet vertices (cf. section 2.2) was originally performed [6] by adopting an algorithm which is equivalent to Furman's one [9], but which is not used anymore in modern phenomenological studies, being infra-red unsafe. In order to use such vertices for the analysis of data from high-energy colliders, we have computed them in the two most popular algorithms: the kt and the cone ones. The ensuing analytical expressions have been taken out in section 4, and the differences among the three algorithms have been highlighted.

The quantitative difference between the small-cone approximations in the kt algorithm and in Furman's one have been estimated in section 5, by plotting several quantities of interest: the jet vertices, the integrand of the high-energy factorization formula, the differential cross section w.r.t. the rapidity distance $Y \equiv |y_1 - y_2|$ of the two MN jets, and some angular coefficients indicating the azimuthal decorrelations of the jets themselves. Also the corresponding quantities with the exact jet vertices in the kt algorithm have been plotted.

It turns out that the difference between the kt and Furman's algorithms is sizeable, of the order of 20% at the level of cross section, and about 5% for the ratios $C_m/C_0 = \langle \cos(m\Delta\phi_J) \rangle$ and C_m/C_n, the angular coefficients of azimuthal decorrelation.

On the other hand, the discrepancies between the exact results and the small-cone approximated ones are much smaller, of the order of 5% at the level of cross section, and less than 2% for the angular ratios. We therefore conclude that the small-cone expansion, computed with the proper jet algorithm, provides a good approximation to the Mueller-Navelet jet vertices; it can then be used as a very convenient tool to perform phenomenological studies, in that it requires much less computational resources than the exact computation.

This aspect could be essential when analysing observables obtained by integrating the jet energies in a non-factorized domain, e.g., by requiring $E_1 + E_2 > 2E_{\text{cut}}$. Such condition is often used in dijet analysis since, at fixed NLO, it yields more stable results than the condition $E_i > E_{\text{min}}$, while retaining the $1 \leftrightarrow 2$ symmetry. On the other hand, a non-factorizable domain of integration in energy prevents the use of eq. (2.22) with independently integrated impact factors $\mathbf{\Psi}$; a numerical integration in energy (and possibly in rapidity) of the integrand (2.20) is thus necessary, and the small-cone approximation represents a valuable tool to reduce the computational effort of such calculation.

JHEP04(2015)071

Acknowledgments

We wish to thank the *Galileo Galilei Institute for Theoretical Physics* where part of this work was performed.

A Expressions of splitting and special functions

The splitting functions found in the jet vertices are defined in the usual way:

$$P_{qq}(z) = C_F \left(\frac{1+z^2}{1-z}\right)_+ = C_F \left[\frac{1+z^2}{(1-z)_+} + \frac{3}{2}\delta(1-z)\right] \tag{A.1a}$$

$$P_{gq}(z) = C_F \frac{1+(1-z)^2}{z} \tag{A.1b}$$

$$P_{qg}(z) = T_R \left[z^2 + (1-z)^2\right] \tag{A.1c}$$

$$P_{gg}(z) = 2C_A \left[\frac{1}{(1-z)_+} + \frac{1}{z} - 2 + z(1-z)\right] + \left(\frac{11}{6}C_A - \frac{n_f}{3}\right)\delta(1-z)\,. \tag{A.1d}$$

The functions I_j are expressed in terms of hypergeometric functions and read [6]

$$\begin{aligned} I_2(n,\gamma,\zeta) = \frac{\zeta^2}{\bar{\zeta}^2}\Bigg[\zeta\Bigg(&\frac{{}_2F_1(1,1+\gamma-\frac{n}{2},2+\gamma-\frac{n}{2},\zeta)}{\frac{n}{2}-\gamma-1} - \frac{{}_2F_1(1,1+\gamma+\frac{n}{2},2+\gamma+\frac{n}{2},\zeta)}{\frac{n}{2}+\gamma+1}\Bigg) \\ &+ \zeta^{-2\gamma}\Bigg(\frac{{}_2F_1(1,-\gamma-\frac{n}{2},1-\gamma-\frac{n}{2},\zeta)}{\frac{n}{2}+\gamma} - \frac{{}_2F_1(1,-\gamma+\frac{n}{2},1-\gamma+\frac{n}{2},\zeta)}{\frac{n}{2}-\gamma}\Bigg) \\ &+ \left(1+\zeta^{-2\gamma}\right)\left(\chi^{(0)}_{n\nu} - 2\log\bar{\zeta}\right) + 2\log\zeta\Bigg] \end{aligned} \tag{A.2a}$$

$$I_{1,3}(n,\gamma,\zeta) = \frac{\bar{\zeta}}{2\zeta} I_2(n,\gamma,\zeta) \pm \frac{\zeta}{\bar{\zeta}}\left[\log\zeta + \frac{1-\zeta^{-2\gamma}}{2}\left(\chi^{(0)}_{n\nu} - 2\log\bar{\zeta}\right)\right] \tag{A.2b}$$

and we recall the definition $\gamma \equiv \mathrm{i}\nu - 1/2$. $\chi^{(0)}_{n\nu}$ is defined in eq. (2.14).

References

[1] A.H. Mueller and H. Navelet, *An Inclusive Minijet Cross-Section and the Bare Pomeron in QCD*, *Nucl. Phys.* **B 282** (1987) 727 [INSPIRE].

[2] A.H. Mueller, *Parton distributions at very small x values*, *Nucl. Phys. Proc. Suppl.* **18C** (1991) 125 [INSPIRE].

[3] A.H. Mueller, *Jets at LEP and HERA*, *J. Phys.* **G 17** (1991) 1443 [INSPIRE].

[4] J. Bartels, D. Colferai and G.P. Vacca, *The NLO jet vertex for Mueller-Navelet and forward jets: The Quark part*, *Eur. Phys. J.* **C 24** (2002) 83 [hep-ph/0112283] [INSPIRE].

[5] J. Bartels, D. Colferai and G.P. Vacca, *The NLO jet vertex for Mueller-Navelet and forward jets: The Gluon part*, *Eur. Phys. J.* **C 29** (2003) 235 [hep-ph/0206290] [INSPIRE].

JHEP04(2015)071

[6] D.Y. Ivanov and A. Papa, *The next-to-leading order forward jet vertex in the small-cone approximation*, *JHEP* **05** (2012) 086 [arXiv:1202.1082] [INSPIRE].

[7] S. Catani, Y.L. Dokshitzer, M.H. Seymour and B.R. Webber, *Longitudinally invariant K_t clustering algorithms for hadron hadron collisions*, *Nucl. Phys.* **B 406** (1993) 187 [INSPIRE].

[8] S.D. Ellis, Z. Kunszt and D.E. Soper, *The One Jet Inclusive Cross-Section at Order α_S^3. 1. Gluons Only*, *Phys. Rev.* **D 40** (1989) 2188 [INSPIRE].

[9] M. Furman, *Study of a Nonleading QCD Correction to Hadron Calorimeter Reactions*, *Nucl. Phys.* **B 197** (1982) 413 [INSPIRE].

[10] B. Jager, M. Stratmann and W. Vogelsang, *Single inclusive jet production in polarized pp collisions at $O(alpha_s^3)$*, *Phys. Rev.* **D 70** (2004) 034010 [hep-ph/0404057] [INSPIRE].

[11] A. Mukherjee and W. Vogelsang, *Jet production in (un)polarized pp collisions: dependence on jet algorithm*, *Phys. Rev.* **D 86** (2012) 094009 [arXiv:1209.1785] [INSPIRE].

[12] F. Caporale, D.Y. Ivanov, B. Murdaca and A. Papa, *Mueller-Navelet small-cone jets at LHC in next-to-leading BFKL*, *Nucl. Phys.* **B 877** (2013) 73 [arXiv:1211.7225] [INSPIRE].

[13] F. Caporale, B. Murdaca, A. Sabio Vera and C. Salas, *Scale choice and collinear contributions to Mueller-Navelet jets at LHC energies*, *Nucl. Phys.* **B 875** (2013) 134 [arXiv:1305.4620] [INSPIRE].

[14] CMS collaboration, *Azimuthal angle decorrelations of jets widely separated in rapidity in pp collisions at $\sqrt{s} = 7$ TeV*, CMS-PAS-FSQ-12-002 (2012).

[15] B. Ducloué, L. Szymanowski and S. Wallon, *Confronting Mueller-Navelet jets in NLL BFKL with LHC experiments at 7 TeV*, *JHEP* **05** (2013) 096 [arXiv:1302.7012] [INSPIRE].

[16] V.N. Gribov and L.N. Lipatov, *Deep inelastic e p scattering in perturbation theory*, *Sov. J. Nucl. Phys.* **15** (1972) 438 [*Yad. Fiz.* **15** (1972) 781] [INSPIRE].

[17] G. Altarelli and G. Parisi, *Asymptotic Freedom in Parton Language*, *Nucl. Phys.* **B 126** (1977) 298 [INSPIRE].

[18] Y.L. Dokshitzer, *Calculation of the Structure Functions for Deep Inelastic Scattering and e^+e^- Annihilation by Perturbation Theory in Quantum Chromodynamics*, *Sov. Phys. JETP* **46** (1977) 641 [*Zh. Eksp. Teor. Fiz.* **73** (1977) 1216] [INSPIRE].

[19] V.S. Fadin, E.A. Kuraev and L.N. Lipatov, *On the Pomeranchuk Singularity in Asymptotically Free Theories*, *Phys. Lett.* **B 60** (1975) 50 [INSPIRE].

[20] E.A. Kuraev, L.N. Lipatov and V.S. Fadin, *Multi-Reggeon Processes in the Yang-Mills Theory*, *Sov. Phys. JETP* **44** (1976) 443 [*Zh. Eksp. Teor. Fiz.* **71** (1976) 840] [*Erratum ibid.* **45** (1977) 199] [INSPIRE].

[21] E.A. Kuraev, L.N. Lipatov and V.S. Fadin, *The Pomeranchuk Singularity in Nonabelian Gauge Theories*, *Sov. Phys. JETP* **45** (1977) 199 [INSPIRE].

[22] I.I. Balitsky and L.N. Lipatov, *The Pomeranchuk Singularity in Quantum Chromodynamics*, *Sov. J. Nucl. Phys.* **28** (1978) 822 [*Yad. Fiz.* **28** (1978) 1597] [INSPIRE].

[23] D. Colferai, F. Schwennsen, L. Szymanowski and S. Wallon, *Mueller Navelet jets at LHC — complete NLL BFKL calculation*, *JHEP* **12** (2010) 026 [arXiv:1002.1365] [INSPIRE].

JHEP04(2015)071